aerospace

MDPI

Article

A Multifidelity Simulation Method for Internal and External Flow of a Hypersonic Airbreathing Propulsion System

Jun Liu [1,*], Huacheng Yuan [1], Jinsheng Zhang [1,2] and Zheng Kuang [1]

[1] College of Energy and Power Engineering, Nanjing University of Aeronautics and Astronautics, Nanjing 210016, China
[2] Shanghai Electro-Mechanical Engineering Institute, Shanghai 201109, China
* Correspondence: liujunnever@nuaa.edu.cn

Abstract: As hypersonic vehicles are highly integrated, a multifidelity simulation method based on a commercial solver is developed to reduce simulation time for such vehicles and their propulsion systems. This method is characterized by high-level fidelity numerical analysis of external flow and low-level fidelity numerical analysis of internal flow. The external flow of a propulsion system is solved by RANS equations. The internal flow is modeled by a quasi-one-dimensional equation. The interaction between external and internal flow is governed by a CFD solver through a user-defined function (UDF). The static pressure distribution acquired from the multifidelity simulation method is in agreement with the experimental data, indicating that this simulation method can be used to study the flow physics of hypersonic propulsion systems at a reasonable cost. From a design perspective, the results indicate that the horizontal force increases with the fuel equivalence ratio, and the thrust balance is realized at $\varphi = 0.35$. The positive net thrust is maintained throughout the flight regime from *Ma* 4 to *Ma* 7, whether the combustor operates in ramjet or scramjet mode.

Keywords: hypersonic airbreathing propulsion system; external and internal flow; quasi-one-dimensional model; multifidelity simulation method

Citation: Liu, J.; Yuan, H.; Zhang, J.; Kuang, Z. A Multifidelity Simulation Method for Internal and External Flow of a Hypersonic Airbreathing Propulsion System. *Aerospace* **2022**, *9*, 685. https://doi.org/10.3390/aerospace9110685

Academic Editor: Qingchun Yang

Received: 10 October 2022
Accepted: 2 November 2022
Published: 3 November 2022

1. Introduction

Scramjet propulsion systems are critical for hypersonic cruise vehicles. To reduce the external drag and improve the lift-to-drag ratio of hypersonic cruise vehicles [1,2], the scramjet propulsion systems are integrated in hypersonic cruise vehicles, consisting of a forebody/inlet [3], combustor [4] and nozzle/afterbody [5]. Although three-dimensional simulations provide more accurate details about the physical flows inside the propulsion system, such simulations are time-consuming. Thus, in order to reduce the simulation time and acquire preliminary results for hypersonic cruise vehicles and propulsion systems in the design process, the quasi-one-dimensional method [6–8] and the multifidelity simulation method [9] are used. The multifidelity simulation method is characterized by external flow field simulated by a CFD code and an internal flow field, which is solved by a quasi-one-dimensional model.

Two methods are available to calculate the flow properties along the combustor. The first is the Heiser–Prattl approach [2], which uses the space-marching method to solve the governing equation. This governing equation takes the combustor area variation and total temperature distribution into account. Smart [10] developed a Mach number distribution ordinary difference equation (ODE) that incorporates wall friction. This normalized ODE is based on isentropic flow equations derived by Shapiro [11]. However, it is difficult to address thermal choke using this method when the Mach number of the flow is unity. To solve the ODE, the core flow area must be prescribed [6]. The other method used to calculate the flow properties is the quasi-one-dimensional unsteady method proposed by Bussing [12], which was developed based on computational fluid dynamic equations

and uses the time-marching method to solve the governing equations. Liu et al. [13] used this method to calculate the unsteady quasi-one-dimensional combustor properties with skin friction, heat dissipation and fuel mixture models. Wang [14] took into account the finite-rate chemical reaction in the combustor model. Compared with the experimental data, Billing [15] and Jiang et al. [16] considered the precombustion shock train in this model and developed a coupling algorithm between the isolator and combustor suitable for dual-mode scramjet.

A multifidelity simulation method of airbreathing propulsion systems has also been investigated. Kim et al. [17] studied the flow field around a N2B hybrid-wing body configuration. The external flow was simulated by a CFD code, and the propulsion system was provided by the NPSS thermodynamic engine cycle model. Their results revealed complex flow physics in the integrated airframe propulsion system. Vijayakumar et al. [18] implemented a quasi-one-dimensional combustor model in a numerical propulsion system simulation (NPSS) and simulated the flow field coupled with FLUENT code. In their work, a compression system a simulated with the FLUENT solver for off-design cases. NPSS and FLUENT were combined in a process coupling method [18]. Complex flow physics were investigated in a dual-mode scramjet engine compression system operating in the range of *Ma* 3.5 to 6.0. Their work demonstrates the importance of multifidelity and component-integrated analysis. Owing to the lack of flame blowout prediction capabilities developed by Vijayakumar et al. [18] and Vu and Wilson [6], Connolly et al. [19] implemented a generalized DMSJ combustors model in NPSS that can identified four operation modes, including unstart, ramjet, scramjet and blowout of the combustor. Based on NPSS, they built a turbine-based combined cycle, which can operate from takeoff to above Mach 5, successfully simulating mode transition from turbomachinery to DMSJ operation.

In this study, we developed a multifidelity simulation method based on a commercial flow solver. The external flow fields of a hypersonic vehicle were calculated using a commercial flow solver, whereas the internal flow of the combustor was calculated using a quasi-one-dimensional model based on the C programming language. The remainder of this paper is organized as follows. First, we introduce the methodology for the proposed multifidelity simulation. Then, we describe the validation of the quasi-one-dimensional combustor model using experimental tests. Then, we explore the external and internal flow fields of a hypersonic vehicle at design points. Finally, we discuss the flow physics and forces at off-design points.

2. Multifidelity Simulation Method

2.1. Computational Fluid Dynamics Solver

A two-dimensional steady state, implicit, density-based ANSYS® FLUENT 14.5 solver was used to solve the fluid flow. The Reynolds-averaged Navier–Stokes (RANS) equations were solved for the inlet and nozzle components of a hypersonic propulsion system. The mass, momentum and energy conservation are expressed in Equations (1)–(3).

Mass conservation equation:

$$\frac{\partial \rho}{\partial t} + \nabla \cdot (\rho \boldsymbol{U}) = 0 \tag{1}$$

Momentum conservation equation:

$$\frac{\partial}{\partial t}(\rho \boldsymbol{U}) + \nabla \cdot (\rho \boldsymbol{U}\boldsymbol{U}) = -\nabla p + \nabla \cdot \tau + \rho \boldsymbol{g} \tag{2}$$

where p is the static pressure, τ is the stress tensor (described below) and $\rho \boldsymbol{g}$ is the gravitational body force.

Energy conservation equation:

$$\frac{\partial}{\partial t}\left[\rho\left(e + \frac{U^2}{2}\right)\right] + \nabla \cdot \left[\rho\left(e + \frac{U^2}{2}\right)\boldsymbol{U}\right] = -p\nabla \cdot \boldsymbol{U} + \nabla \cdot (\lambda \nabla T) + \Phi + S_h \tag{3}$$

where λ is the effective conductivity, Φ is the dissipation function and S_h represents volumetric heat sources.

These equations are discretized with a finite volume method. The implicit solution formulation is selected. A Roe flux-difference splitting (Roe-FDS) scheme is used to discretized the convective fluxes. The viscid flux is discretized based on a second-order central difference scheme. The one-equation S-A equation is used to model the turbulent flow. The fluid is treated as compressible ideal gas. The molecular viscosity of the gas is calculated using Sutherland's law, with three coefficients defined as:

$$\mu = \mu_0 \left(\frac{T}{T_0} \right)^{3/2} \frac{T_0 + S}{T + S} \tag{4}$$

where the reference viscosity (μ_0) and reference temperature (T_0) are 1.716×10^{-5} kg/ms^{-1} and 273.11 K, respectively, and the effective temperature (S) is 110.56 K.

2.2. Quasi-One-Dimensional Flow Model

The combustor component is modeled by a quasi-one-dimensional flow conservation Equation (5), which accounts for mass addition, area variable, wall friction and heat release. These factors are included in the source term $\boldsymbol{J}$.

$$\frac{\partial \boldsymbol{U}}{\partial t} + \frac{\partial \boldsymbol{F}}{\partial x} = \boldsymbol{J} \tag{5}$$

where $\boldsymbol{U}$ is the solution vector, and $\boldsymbol{F}$ and $\boldsymbol{J}$ are the flux vector and the source term, respectively, defined as follows:

$$\boldsymbol{U} = \begin{bmatrix} \rho A \\ \rho A U \\ \rho(e + U^2/2)A \end{bmatrix}, \boldsymbol{F} = \begin{bmatrix} \rho A U \\ \rho A U^2 + pA \\ \rho(e + U^2/2)AU + pAU \end{bmatrix}, \boldsymbol{J} = \begin{bmatrix} \frac{d\dot{m}_f}{dx} \\ p\frac{\partial A}{\partial x} - \frac{\rho U^2}{2} f \cdot C_{\text{wet}} \\ \frac{d\dot{Q}}{dx} \end{bmatrix} \tag{6}$$

where $d\dot{m}_f$ is the fuel mass flow rate; f is the combustor wall friction coefficient, ranging from 0.003 to 0.005 and set to 0.003 in this study; C_{wet} is the combustor wet perimeter; and $d\dot{Q}$ is cumulative heat release. The cumulative heat release distribution schedule is determined by a power law relationship using the non-dimensional length along the combustor [20]:

$$Q(x) = Q_{\max} \left(\frac{x}{L_c} \right)^{\frac{1}{3}} \tag{7}$$

where $Q_{\max} = f_{st} H_{prop}$, f_{st} is the stoichiometric ratio, H_{prop} is the heat value and L_c is the length of combustor.

The quasi-one-dimensional conservation equations are solved by a MacCormack numerical scheme [21], which is a two-step, second-order-accurate (in both time and space), explicit finite-difference method. The forward-difference scheme is used to calculate the spatial discretization in the predictor step:

$$\overline{\boldsymbol{U}}_i^n = \boldsymbol{U}_i^n - \frac{\Delta t}{\Delta x} \left(\boldsymbol{F}_{i+1}^n - \boldsymbol{F}_i^n \right) + \Delta t \boldsymbol{J}_i^n \tag{8}$$

The backward-difference scheme is used in the corrector step:

$$\boldsymbol{U}_i^{n+1} = \frac{1}{2} \left[\boldsymbol{U}_i^n + \overline{\boldsymbol{U}}_i^n - \frac{\Delta t}{\Delta x} \left(\boldsymbol{F}_i^{n+1} - \boldsymbol{F}_{i-1}^{n+1} \right) + \Delta t \boldsymbol{J}_i^{n+1} \right] \tag{9}$$

where superscript n represents time ($t = n\Delta t$), and subscript i refers to the spatial grid point (x_i). The time step is determined based on the numerical stability equation:

$$\Delta t \leq \mathrm{CFL}\frac{\Delta x}{V + a} \tag{10}$$

where the CFL value must be less than or equal to 1.0 for the MacCormack scheme be stable.

To damp out numerical oscillations in the vicinity of large gradients, artificial viscosity is introduced in the MacCormack method. The artificial viscosity applied to the conservation equations is defined as:

$$\boldsymbol{S}_i^n = Nu\frac{\left|p_{i+1}^n - 2p_i^n + p_{i-1}^n\right|}{p_{i+1}^n + 2p_i^n + p_{i-1}^n}(\boldsymbol{U}_{i+1}^n - 2\boldsymbol{U}_i^n + \boldsymbol{U}_{i-1}^n) \tag{11}$$

where Nu is an adjustable viscosity-like constant. The value of Nu varies from 0.01 to 0.3; we selected $Nu = 0.1$ based on the accuracy of the final solution.

To solve the quasi-one-dimensional equations, the upstream and downstream boundary conditions need to be specified. There are two types of flow at these two boundaries, depending on the direction of three characteristics ($\boldsymbol{U} + a$, $\boldsymbol{U} - a$, a). For the supersonic condition, all three characteristics point toward the upstream boundary and away from the downstream boundary. For the subsonic condition, one characteristic ($\boldsymbol{U} - a$) points toward the upstream and away from the downstream boundary.

The combustor can operate in ramjet or scramjet mode; therefore, the upstream boundary condition of the combustor is subsonic or supersonic under the upstream boundary conditions. Under supersonic conditions, the values of three conservation variables are calculated based on the upstream total pressure, total temperature and Mach number. For subsonic conditions, the static pressure is determined based on the combustor model. The first two conservation variables, $\boldsymbol{U}_1$ and $\boldsymbol{U}_2$, are extrapolated from the upstream boundary and used in combination with specific static pressure to calculate $\boldsymbol{U}_3$.

In this study, only supersonic downstream boundary conditions were considered. The three conservation variables were extrapolated from interior points, which are defined as followed:

$$\boldsymbol{U}_{i\ \mathrm{exit}} = 2\boldsymbol{U}_{i\ \mathrm{exit}-1} - \boldsymbol{U}_{i\ \mathrm{exit}-2} \tag{12}$$

2.3. Coupling of the Quasi-One-Dimensional Model and CFD Codes

The coupling procedure between the combustor and inlet/nozzle components is illustrated in this section. A schematic diagram of a hypersonic vehicle is shown in Figure 1. The hypersonic airbreathing propulsion system comprises three main components: a forebody/inlet, combustor and nozzle/afterbody. The inlet and nozzle components are solved with two-dimensional RANS equations. A mass-weighted average is used to calculate the flow quantities at the interfaces [22], which is defined as:

$$\overline{\phi} = \frac{\int \rho\phi dA}{\int \rho dA} \tag{13}$$

where ρ is the density, ϕ is any conserved quantity to be one-dimensionalized, A is the area over which the average is performed and $\overline{\phi}$ represents flow quantity after mass-weighted averaging.

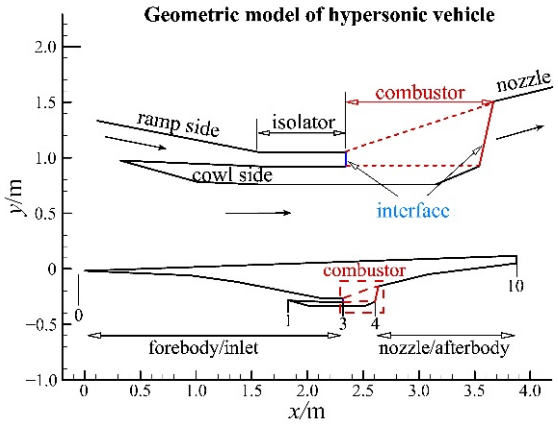

Figure 1. Schematic diagram of a hypersonic vehicle.

The coupling procedure of this multifidelity simulation is illustrated in Figure 2.

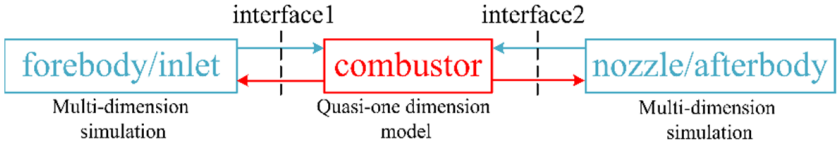

Figure 2. Coupling procedure of the multifidelity simulation method.

(1) Solve 2D RANS equations and acquire the initial external flow fields;
(2) Calculate the mass-weighted average quantities at the interfaces;
(3) Solve the quasi-one-dimensional equation based on the upstream and downstream boundary conditions of the combustor;
(4) Update the values at the interfaces and recompute the external flow fields; and
(5) If the iteration converges, then stop; otherwise, return to step (1).

The flow field of a hypersonic vehicle with a propulsion system is investigated based on previously introduced multifidelity simulation method. A schematic diagram of this vehicle is shown in Figure 1, and the detailed dimensions the hypersonic propulsion system are listed Table 1. As mentioned previously, the inlet and nozzle are solved with a CFD solver; the mesh and boundary conditions are shown in Figure 3. ICEM software is used to generate the mesh, and local refinement is conducted for regions with significant velocity gradients, such as in the vicinity of shock waves and wall. The inflow is set as a pressure far-field boundary condition. The outflow is set as a pressure outlet. The entrance and exit of the combustor are set as pressure outlet and pressure inlet boundary conditions, respectively. The quasi-one-dimensional combustor model is implemented in the FLUENT solver by a user-defined function.

Table 1. Geometric properties of the investigated hypersonic vehicle.

Property	Value	Property	Value
Inlet length (m)	2.13	Capture height(m)	0.27
Isolator length (m)	0.187	Throat height(m)	0.03
Combustor length (m)	0.32	Total contraction ratio	8.76
Nozzle length (m)	0.124	Combustor area ratio	4.63
Ramp angles	2.5°, 5.5° and 3°	Nozzle expansion ratio	2.49

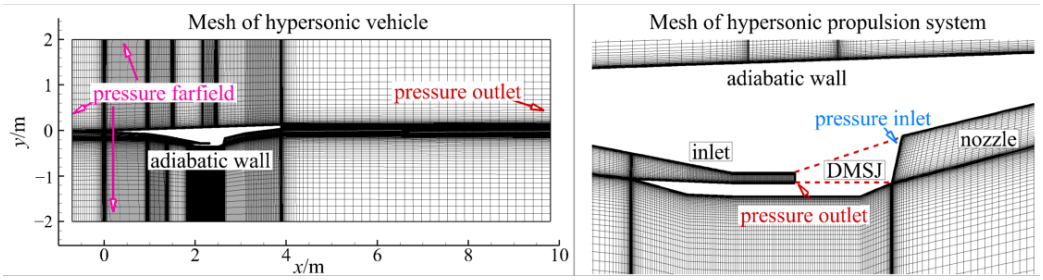

Figure 3. Mesh and boundary conditions of the investigated hypersonic vehicle.

2.4. Validation

The quasi-one-dimensional simulation method adopted in this study was verified by the University of Virginia combustor experiment tests [23]. A schematic representation of the experimental model is shown in Figure 4. This model is installed on the direct connected facility and consists of a Laval nozzle, isolator, combustor and diffuser. The combustor can be split into two sections, each of which is made up of rectangular tubes with a constant cross-section and single expansion diffuser. Hydrogen is selected as the fuel and injected through a 10° ramp. The experimental model is non-dimensional with respect to the injector ramp height (h). During the test, the temperature at the isolator entrance is 1160 K, total pressure is 330 kPa, the Mach number is 2.03 and the fuel equivalence ratio (φ) varies from 0 to 0.31. Test results with a fuel equivalence ratio of 0 and 0.21 are used to verify the simulation method developed in this study, and the flow properties at the entrance of the combustor are shown in Table 2.

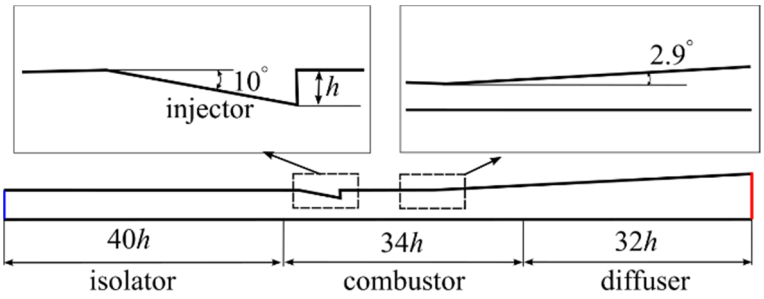

Figure 4. Schematic representation of the experimental model.

Table 2. Flow Properties at the entrance of combustor after mass-weighted averaging.

φ	*Ma*	*P* (kPa)	*T* (K)	*Pt* (kPa)	*Tt* (K)
0	1.81	49.09	617.1	298.93	1020.0
0.21	0.9871	129.75	848.75	257.62	1020.0

The static pressure distribution along the flow path between experimental tests and multifidelity simulation at varying fuel equivalence ratios are shown in Figure 5. The square symbols represent the experimental tests, and solid lines represent the simulation results. As shown in the figure, the pressure distribution obtained in multifidelity simulations are in agreement with the experimental test results. The pressure fluctuates at the entrance of the combustor when the combustor is powered off ($\varphi = 0$) because the geometry of the injector is not considered during multifidelity simulations. During the test, the inflow is supersonic, and oblique shock is induced from the injector ramp. When the combustor operates at $\varphi = 0.21$, the simulation results are in agreement with the test results, including those for the starting location of the shock train [24] and the maximum static pressure along the internal flow path. Therefore, the multifidelity simulations method introduced above is sufficiently accurate for further investigation.

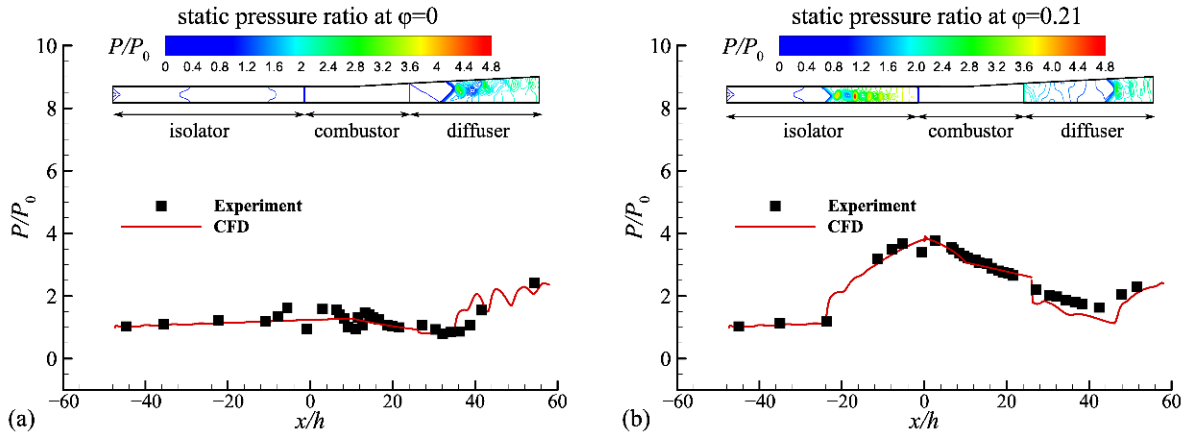

Figure 5. Multifidelity simulations compared to wind tunnel tests. (**a**) Static pressure distribution along the combustor and pressure contour at a fuel equivalence ratio of 0; (**b**) static pressure distribution along the combustor and pressure contour at a fuel equivalence ratio of 0.21.

3. Results

3.1. Design Point

The flow field of an integrated hypersonic vehicle was investigated based on the multifidelity simulation method presented above. In this section, we discuss the design point results of the simulation.

The Mach number contour and static pressure ratio along the ramp side of hypersonic vehicle at varying fuel equivalence ratios are shown in Figure 6. In Figure 6c, the blue solid line with triangular symbols represents the combustor power-off mode, and the red solid line with rectangular symbols represents the fuel equivalence ratio at 0.60. The static pressure distribution at these two fuel equivalence ratios remains the same until the isolator. With the combustor power off (Figure 6a), there is no shock train in the isolator, and the oblique shock waves reflect between the ramp side and the cowl side of the vehicle which, causing static pressure fluctuation (Figure 6c). With the combustor power on, an oblique shock train forms in the isolator, as shown in Figure 6b, as a result of the high backpressure in the combustor. The static pressure increases sharply, and part of the flow speed decelerates to the subsonic level and flows into the combustor.

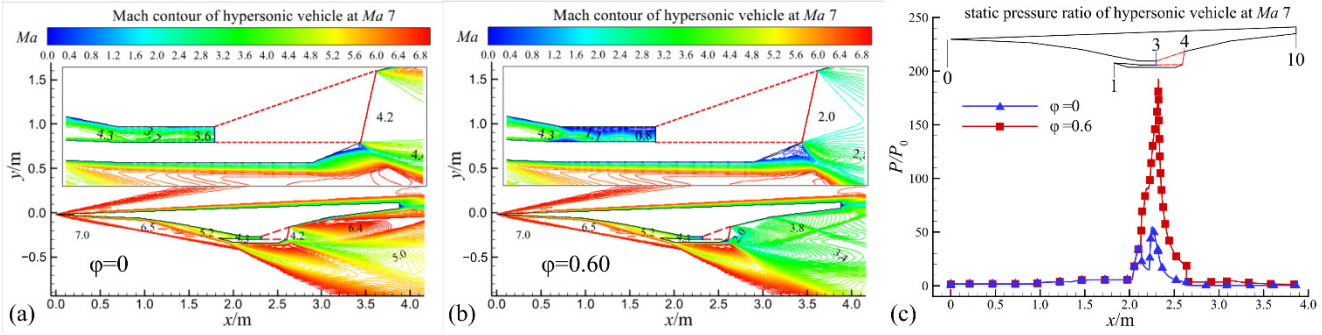

Figure 6. Mach contour and static pressure of the investigated hypersonic vehicle at *Ma* 7. (**a**) External and internal flow at a fuel equivalence ratio of 0; (**b**) external and internal flow at a fuel equivalence ratio of 0.60; (**c**) static pressure distribution along the flow path at two different fuel equivalence ratios.

The profiles of flow quantities passed on to the quasi-one-dimensional combustor model are shown in Figure 7. The total temperature, total pressure, Mach number and mass flow rate determined by the CFD solver are mass-weight-averaged and passed on to the combustor. The flow quantities along the combustor are presented in Figure 8, with the combustor power on and operating at a fuel equivalence ratio of 0.60. As shown in Figure 8,

a thermal choke forms at axis position x = 2.35 m. The Mach number decreases from the entrance of the combustor until the thermal choke and then increases gradually, owing to the diffusion of the combustor flow path. The temperature increases significantly at the beginning of the combustor and then increases gradually until the end of the combustor.

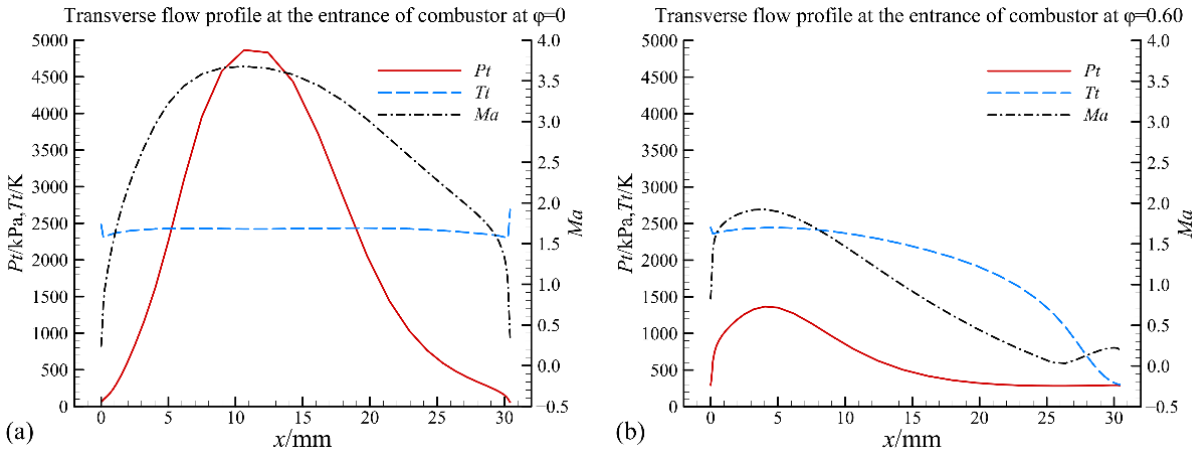

Figure 7. Transverse flow profile at the entrance of the combustor. (**a**) Flow quantities at the entrance of combustor at a fuel equivalence ratio of 0; (**b**) flow quantities at the entrance of the combustor at a fuel equivalence ratio of 0.6.

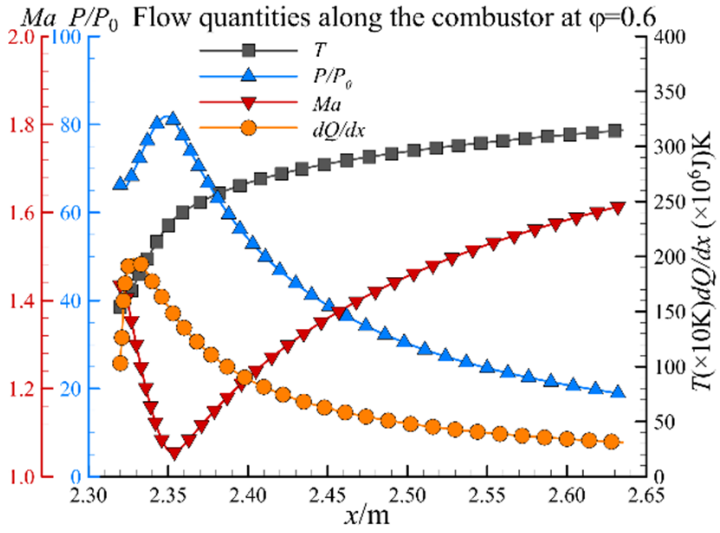

Figure 8. Flow quantities along the combustor at φ = 0.60.

The flow quantities, including temperature, static pressure ratio, Mach number and heat release profile along the combustor are shown in Figure 8. Here, we discuss the flow properties at varying fuel equivalence ratios. The Mach numbers along the combustor at a fuel equivalence ratios in the range of 0 to 0.6 are shown in Figure 9. With the combustor power off, the Mach number along the flow path increases gradually, owing to the divergence of the combustor chamber. The Mach number at the end of combustor decreases from 4.0 to 1.2 with the fuel equivalence ratio. The combustor operates in scramjet mode when the fuel equivalence ratio is less than 0.5. As the fuel equivalence ratio increases further, a thermal choke occurs, and the combustor operation mode progressively shifts from scramjet to ramjet.

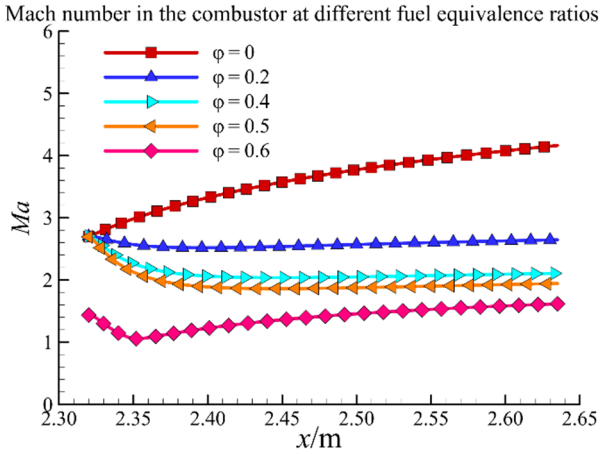

Figure 9. Mach number along the combustor at fuel equivalence ratios in the range of 0 to 0.6.

The flow properties at different stations of the hypersonic vehicle are summarized in Table 3 according to the previously calculated external and internal flow fields. The horizontal and vertical force coefficients at fuel equivalence ratios ranging from 0 to 0.60 are shown in Figure 10, with horizontal force and vertical force coefficients defined as:

$$c_x = \frac{F_x}{1/2\rho U^2 A_0}, c_y = \frac{F_y}{1/2\rho U^2 A_0} \tag{14}$$

Table 3. Station flow properties at design points.

φ	Station	*Ma*	*P* (kPa)	*T* (K)	*Pt* (kPa)	*Tt* (K)
0	0	7.0	1.6	224.5	6736.4	2419.4
	3	3.12	50.9	856.2	2908.5	2419.4
	4	4.16	5.40	534.2	1019.3	2382.1
	10	6.09	0.60	293.4	931.5	2382.1
0.6	3	1.37	233.9	1548.9	872.5	2419.4
	4	1.97	30.1	2022.9	223.2	3581.2
	10	3.47	2.8	1058.8	202.4	3578.1

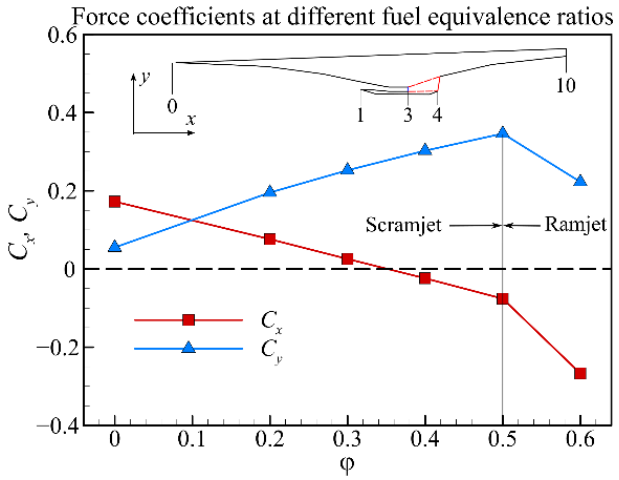

Figure 10. Horizontal and vertical force coefficients at fuel equivalence ratios in the range of 0 to 0.6.

The horizontal and vertical forces containing pressure and skin friction terms are integrated from the external and internal surfaces of the hypersonic vehicle. The horizontal force coefficient is positive at φ = 0, which represents the drag with the combustor power

off. The horizontal force coefficient decreases linearly with the fuel equivalence ratio until φ = 0.5. The horizontal force coefficient is zero at φ = 0.35, which indicates that the thrust produced by the propulsion system is equal to the drag of the vehicle at this fuel equivalence ratio. Beyond this point, the thrust is greater than the drag. The deflection of the horizontal force coefficient is the result of the operation condition of the combustor, which switches from scramjet to ramjet mode (Figure 9). The vertical force coefficient, which indicates the lift of the hypersonic vehicle, increases with the fuel equivalence ratio. It increases linearly when the combustor operates in scramjet mode, corresponding to the horizontal force coefficient.

3.2. Off-Design Points

The flow fields and quantities at the design points of the hypersonic vehicle are investigated above. In this section, we discuss the flow fields and quantities at the off-design points. The flow fields of the hypersonic vehicle for inflow Mach 4 to 6 are presented in Figure 11. The fuel equivalence ratios at these points are 0.5. The operation of the combustor can be classified as ramjet or scramjet mode according to the Mach number at the exit of the isolator. The Mach number at the exit of the isolator is lower than 1.0 in the range of Mach 4.0 to 5.5, indicating that the combustor is operating in ramjet mode. As the inflow Mach number increases to *Ma* 6, the operation mode of combustor switches to scramjet mode.

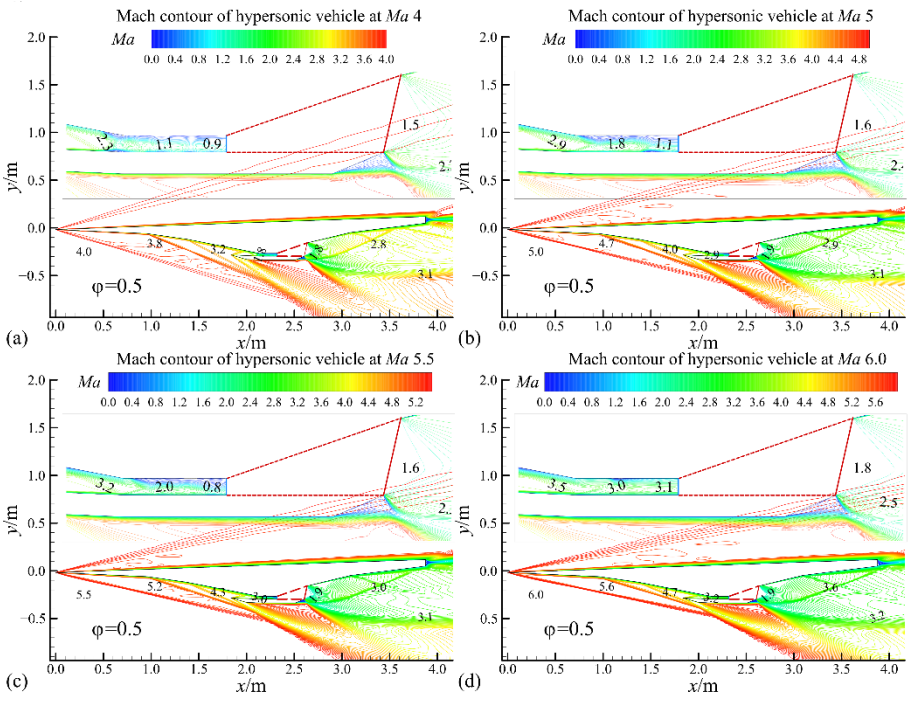

Figure 11. Mach contour of the hypersonic vehicle at off-design points from inflow Mach number 4 to 6. (**a**) Mach contour of the hypersonic vehicle at inflow Mach number 4.0; (**b**) Mach contour of the hypersonic vehicle at inflow Mach number 5.0; (**c**) Mach contour of the hypersonic vehicle at inflow Mach number 5.5; (**d**) Mach contour of hypersonic vehicle at inflow Mach number 6.0.

The static pressure ratios of ramjet and scramjet mode are shown in Figure 12. The static pressure increases with oblique shocks from ramps. Significant pressure increases in the inlet isolator as a result of shock trains. The shock train structure obvious in ramjet mode. As the inflow Mach number increases up to *Ma* 6, the Mach number at the exit of the isolator is supersonic, and the combustor operates in scramjet mode.

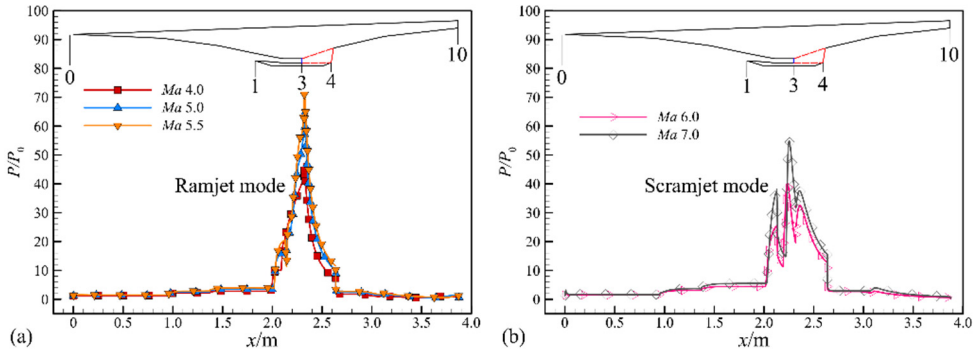

Figure 12. Static pressure ratios at off-design points from Mach 4 to 6. (**a**) Static pressure ratio of the hypersonic vehicle in ramjet mode; (**b**) static pressure ratio of the hypersonic vehicle in scramjet mode.

Analysis of the flow field and static pressure ratio distribution provides basic knowledge about the flow physics at off-design points. Here, we further investigate the combustor. The temperature and Mach number along the combustor at the off-design points are shown in Figure 13. In this figure, the solid symbols represent ramjet mode, and the open symbols represent scramjet mode. In ramjet mode, the temperature increases significantly at the beginning of the combustor and then increases mildly until the end of the combustor. The maximum temperature increases with the inflow Mach number. The Mach number first decreases and then increases until the end of the combustor. In scramjet mode, the temperature distribution law is similar to that in ramjet mode, although the temperature at the entrance of the combustor is lower than in ramjet mode. In scramjet mode, the Mach number decreases with the significant heat release at the beginning of the combustor and then remains almost constant until the end of the combustor as a result of area diffusion and heat release.

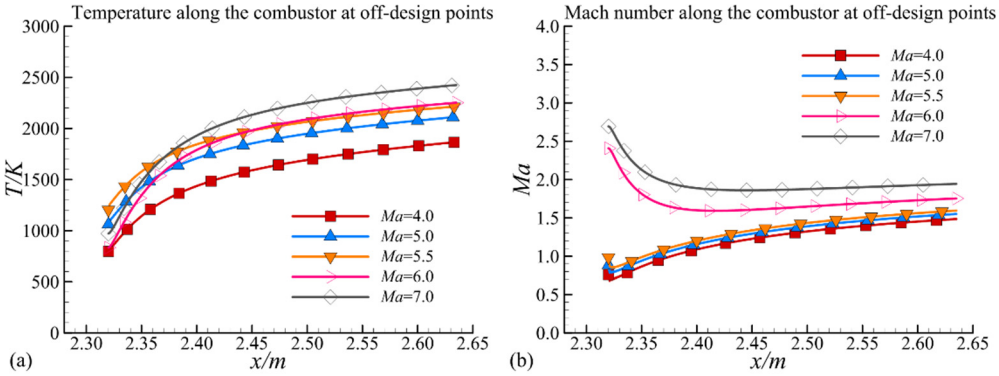

Figure 13. Temperature and Mach number along the combustor from Mach number 4 to 7. (**a**) Temperature of the hypersonic vehicle from Mach number 4 to 7; (**b**) Mach number of the hypersonic vehicle from Mach number 4 to 7.

The horizontal and vertical force coefficients at inflow Mach numbers from 4 to 7 are shown in Figure 14 according to the previously external and internal flow fields. The horizontal and vertical forces, including pressure and viscous terms, are integrated from the external and internal surfaces of the hypersonic vehicle. The horizontal force coefficient is negative withing this Mach number range, indicating that the propulsion system can produce net thrust. The net thrust coefficient is approximately 0.3 in ramjet mode and decreases to approximately 0.1 in scramjet mode. The vertical force coefficient is between 0.2 and 0.3, except at *Ma* 5.5, at which point the combustor operation mode switches from ramjet to scramjet.

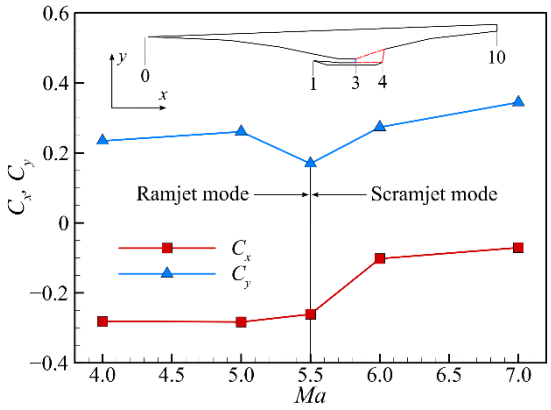

Figure 14. Horizontal and vertical force coefficients at varying Mach numbers.

4. Conclusions

A multifidelity simulation method was developed based on a quasi-one-dimensional combustor model with a commercial solver. This multifidelity simulation method was used to analyze external and internal flow physics of a hypersonic vehicle. The following conclusion can be drawn:

(1) A multifidelity simulation method characterized by high-level fidelity numerical analysis of the inlet and nozzle components and low-level fidelity numerical analysis of the combustor was developed based on a user-defined function and a commercial solver. According to the validation with directed connect wind tunnel tests, the static pressure distribution along the flow path is in agreement with experimental data, indicating that this simulation method can be used to study the flow physics of hypersonic propulsion systems at a low cost.

(2) The proposed multifidelity simulation method can be used for integration analysis of external and internal flow physics of hypersonic propulsion systems at design and off-design points. The design point results indicate that the combustor operation condition varies with the fuel equivalence ratio and operates in scramjet mode until $\varphi = 0.60$. The horizontal force increases with the fuel equivalence ratio, and thrust balance is achieved at $\varphi = 0.35$.

(3) The off-design point results indicate that the combustor operates in ramjet mode from inflow Mach number 4.0 to 5.5 and then switches to scramjet mode. The static pressure, temperature and Mach number distributions along the combustor differ between ramjet and scramjet modes, resulting in net thrust produced by the propulsion system. The net thrust is positive during the whole flight regime between inflow Mach numbers 4 to 7, and the horizontal force coefficient is approximately 0.3 in ramjet mode, then decreasing to 0.1 in scramjet mode.

Author Contributions: Conceptualization, J.L. and H.Y.; methodology, J.L.; software, J.L.; validation, J.Z.; formal analysis, Z.K.; investigation, J.L.; resources, J.L.; data curation, Z.K.; writing—original draft preparation, J.L.; writing—review and editing, J.L. and H.Y.; visualization, J.L. and J.Z.; supervision, H.Y.; project administration, H.Y.; funding acquisition, J.L. and H.Y. All authors have read and agreed to the published version of the manuscript.

Funding: This research was funded by the Fundamental Research Funds for the Central Universities (NS20220024), the Science Center for Gas Turbine Project (P2022-B-I-004-001), the National Natural Science Foundation of China (11772155) and the Aeronautical Science Foundation of China (20200012052001).

Data Availability Statement: Not applicable.

Conflicts of Interest: The authors declare no conflict of interest.

References

1. Walker, B.; Kennedy, K.; Mikkeison, C. US army hypersonic scramjet propelled missile technology program. In Proceedings of the 14th AIAA/AHI Space Planes and Hypersonic Systems and Technologies Conference, Canberra, Australia, 6–9 November 2006; AIAA Paper 2006-7927.
2. Heiser, W.H.; Pratt, D.T.; Daley, D.; Mehta, U. *Hypersonic Airbreathing Propulsion*; AIAA Education Series; AIAA: Washington, DC, USA, 1994; pp. 346–370.
3. Yuan, H.C.; Liu, J.; Zhang, J.S.; Wang, Y. The design and validation of over/under turbine-based combined cycle inlet. *Aerosp. Sci. Technol.* **2020**, *105*, 105960. [CrossRef]
4. Wang, Y.H.; Song, W.Y. Experimental investigation of influence factors on flame holding in a supersonic combustor. *Aerosp. Sci. Technol.* **2019**, *85*, 180–186. [CrossRef]
5. Yu, K.K.; Xu, J.L.; Lv, Z.; Song, G. Inverse design methodology on a single expansion ramp nozzle for scramjets. *Aerosp. Sci. Technol.* **2019**, *92*, 9–19. [CrossRef]
6. Vu, L.N.; Wilson, D. Quasi-one-dimensional scramjet combustor flow solver using the numerical propulsion system simulation. In Proceedings of the 2018 Joint Propulsion Conference, Cincinnati, OH, USA, 9–11 July 2018; AIAA paper 2018-4843.
7. Cao, R.; Lu, Y.; Yu, D.; Chang, J. Study on influencing factors of combustion mode transition boundary for a scramjet engine based on one-dimensional model. *Aerosp. Sci. Technol.* **2020**, *96*, 105590. [CrossRef]
8. Tian, L.; Chen, L.H.; Chen, Q.; Li, F.; Chang, X.Y. Quasi-one-dimensional multimodes analysis for dual-mode scramjet. *J. Propul. Power* **2014**, *30*, 1559–1567. [CrossRef]
9. Lytle, J. Multi-fidelity simulations of air breathing propulsion systems. In Proceedings of the 42nd AIAA/ASME/SAE/ASEE Joint Propulsion Conference & Exhibit, Sacramento, CA, USA, 9–12 July 2006; AIAA paper 2006-4967.
10. Smart, M.K. Scramjets. *Aeronaut. J.* **2007**, *111*, 605–619. [CrossRef]
11. Shapiro, A.H.; Shapiro, R.E. *The Dynamics and Thermodynamics of Compressible Fluid Flow*; Wiley: Hoboken, NJ, USA, 1953; Volume 1, pp. 219–238.
12. Bussing, R.T.A.; Murman, E.M. A one-dimensional unsteady model of dual mode scramjet operation. In Proceedings of the 21st Aerospace Sciences Meeting, Reno, NV, USA, 10–13 January 1983; AIAA paper 83-0422.
13. Liu, J.H.; Ling, W.H.; Liu, X.Z.; Liu, L.; Zhang, Z. A quasi-one dimensional unsteady numerical analysis of supersonic combustor performance. *J. Propul. Technol.* **1998**, *19*, 1–6. (In Chinese)
14. Wang, L. *The Numerical Simulation of the Combustor of Scramjet*; Northwestern Polytechnical University: Xi'an, China, 2011. (In Chinese)
15. Billig, F.S. Research on supersonic combustion. *J. Propul. Power* **1993**, *9*, 499–514. [CrossRef]
16. Jiang, J.; Chu, M.; Xu, X. A quasi-one-dimensional method for prediction of dual mode scramjet combustor performance. *J. Propul. Technol.* **2013**, *34*, 802–808. (In Chinese)
17. Kim, H.; Liou, M.S. Flow simulation of N2B hybrid wing body configuration. In Proceedings of the 50th AIAA Aerospace Sciences Meeting including the New Horizons Forum and Aerospace Exposition, Nashville, TN, USA, 9–12 January 2012; AIAA paper 2012-0838.
18. Vijayakumar, N.; Wilson, D.R.; Lu, F.K. Multifidelity simulation of a dual mode scramjet compression system using coupled NPSS and FLUENT codes. In Proceedings of the 50th AIAA/ASME/SAE/ASEE Joint Propulsion Conference, Cleveland, OH, USA, 28–30 July 2014; AIAA paper 2014-3845.
19. Connolly, B.J.; Krouse, C.; Musgrove, G.O. Implementing a dual-mode scramjet combustor model in NPSS. In Proceedings of the AIAA Propulsion and Energy Forum 2021, Virtual, 9–11 August 2021; AIAA paper 2021-3538.
20. Riggins, D.; Tackett, R.; Taylor, T. Thermodynamic analysis of dual-mode scramjet engine operation and performance. In Proceedings of the 14th AIAA/AHI International Space Planes and Hypersonics Systems and Technologies Conference, Canberra, Australia, 6–9 November 2006; AIAA paper 2006-8059.
21. Anderson, J.D. *Computational Fluid Dynamics*; McGraw-Hill Science; Springer: Berlin/Heidelberg, Germany, 2010; pp. 153–155.
22. Baurle, R.A.; Gafney, R.L. Extraction of one-dimensional flow properties from multidimensional data sets. *J. Propul. Power* **2008**, *24*, 704–714. [CrossRef]
23. Le, D.B.; Goyne, C.P.; Krauss, R.H.; McDaniel, J.C. Experimental study of a dual-mode scramjet isolator. *J. Propul. Power* **2008**, *24*, 1050–1057. [CrossRef]
24. Shi, W.; Chang, J.; Zhang, J.; Ma, J.; Wang, Z.; Bao, W. Numerical investigation on the forced oscillation of shock train in hypersonic inlet with translating cowl. *Aerosp. Sci. Technol.* **2019**, *87*, 311–322. [CrossRef]